The Remanufacturing Process and Performance of ZM6 Alloy Gearbox by Laser Cladding

Weibin Ren (renweibin100@163.com)
Jiangsu University of Technology
Wu Ruiyu
Wu Peng
Wang Yujiang
Ren Yuzhong
Li Yaping

Research Article

Keywords: remanufacturing, laser cladding, ZM6 alloy, gearbox

Posted Date: February 11th, 2022

DOI: https://doi.org/10.21203/rs.3.rs-1311447/v1

Abstract

In view the fact that the excessive element burning, the powder deflagration and the loose structure of the ZM6 alloy gearbox through laser cladding process, the process and method of homogeneous alloy coating prepared by laser cladding under ultra-low oxygen content was proposed, the good microstructure and mechanical properties of the remanufactured part were verified. The experiment results show that, there are no internal defects such as loose or gas hole in the laser remanufactured zone, the microstructure fineness density of the remanufactured part is close to the original substrate, the element difference is relatively small. The contents of Mg, Zr, Nd, Zn and other major elements remain basically constant. The coating and substrate are mainly composed of equiaxed crystalline grains. The crystalline grains of the coating are obviously finer than those of the substrate, further the precipitation of granular or microspherical intragranular and intergranular strengthening phases is more dispersed and uniform, which is mainly composed of α-Mg and β-$Mg_{12}Nd$ phase composition. There is no obvious coarsening in the heat affected zone. The microhardness from the top layer to the interface is between 56.4~63.2 $HV_{0.1}$, The microhardness of the heat affected zone is between 54.2~56.4 $HV_{0.1}$, which are higher than that of other parts of the substrate. The maximum bending load borne of the coating is between 152~167 N, the bending strength is distributed between 205~220 MPa, and the friction coefficient of the coating is distributed between 0.26~0.42. The relevant mechanical properties are meet the remanufacturing standards.

1. Introduction

ZM6 alloy is Mg-Nd-Zn-Zr magnesium alloy. Because of its low density characteristics and good specific strength, shock absorption and impact resistance, it is widely used in the rear gearbox of aircraft engine, aircraft hydraulic constant speed device support, wing rib and other structures[1–3]. This kind of structural parts are mainly manufactured by sand casting, but the casting is prone to produce defects such as porosity, shrinkage cavity, slag inclusion, sand inclusion and etc[4–5]. In order to reduce the remelting rate of this kind of structural parts, defect repair welding has become the main process method to solve this problem.

In view of the difficulties above, scholars at home and abroad have been carried out relevant researches. Miroslav Sahul and other scholars [6] carried out research on the effects of macro and micro structures, mechanical properties and oxide layer on the properties of welded joints after laser welding AZ31 alloy. Wahba and other scholars [7] used laser equipment to realize the welding of AZ91D alloy and non-metallic materials. Gao and other researchers [8] prepared aluminum-copper coating on AZ91HP alloy by wide beam laser cladding, which effectively strengthened the hardness, wear resistance and corrosion resistance of the alloy. Zheng Yi [9] provided the basis for the service requirements of ZM6 magnesium alloy after repair welding through studying the microstructure and properties of ZM6 alloy after repair welding. Wang Xin [10] realized the repair of ZM6 alloy castings by studying and optimizing the TIG wire filling repair welding process parameters, and analyzed the causes of repair joint cracks. Through studying the cladding materials and process parameters on the influence of the defects, Li Xiaoxi and his

team members [11] effectively reduced the defects of laser cladding layer. However, there are still some relative limitations in the researcher above.

(1) There are few studies on the process and properties of laser additive remanufacturing of homogeneous magnesium alloy. The additive remanufacturing of non-homogeneous alloy is difficult to ensure the coating and interface properties, and there are differences in microstructure and properties between the original part and the remanufactured part.

(2) The ignition point of ZM6 alloy is low, the cladding alloy power burns violently during the cladding process, which is difficult to realize the remanufacture process of three-dimensional forming. Further, there are few related studies of processes and methods about this.

(3) The defects of pores and cracks in ZM6 alloy metal remanufacturing cladding are difficult to control, the phenomenon of coarse grain is obvious, which is difficult to ensure the structural excellence of the regenerated coating.

Above all, the laser cladding of homogeneous magnesium alloy was adopt to remanufacture ZM6 gearbox in this research. The formation of good microstructure and mechanical properties of coating under ultra-low oxygen content was realized. The relevant research and process methods provided process and method references for the laser remanufacture of magnesium alloy parts.

2 The Laser Cladding Process

2.1 Technical difficulties and Strategies

In the experiment, the ZM6 alloy gearbox with casting porosity inside was used as the substrate, the homogeneous magnesium alloy with the same element type and content is used as the cladding power. The application of the same composition alloy cladding material is to ensure the formation of good performance of cladding interface. The material compositions are shown by Tab.1. There are the following process difficulties of the laser remanufacture.

(1) The existence of oxygen content in laser remanufacturing process environment could aggravate the burning loss of active elements in the alloy, even cause severe combustion of the alloy powder.

(2) Due to the low melting point and ignition point of ZM6 alloy, the relatively low laser power should be selected in the remanufacturing process. While the relatively low laser power is difficult to form the metallurgical bonding between the cladding layer and the substrate. So the laser cladding process window for ZM6 alloy remanufacture is narrow.

(3) There are some refractory metal elements in ZM6 alloy, such as zirconium. Under the relatively low laser power process, some zirconium elements could disperse above the forming area, which form the metal dust or roll into the molten pool to form cladding slag inclusion.

(4) In the process of laser cladding forming, the ZM6 alloy power is easy to form liquefaction cracks or ductile cracks, resulting in forming failure or coating quality degradation.

In view of the forming difficulties above, the following process strategies are formulated.

(1) The laser cladding process is carried out in the inert gas protection chamber. The oxygen and other gases contained in the chamber are discharged through the injection of argon, in order that the oxygen content in the chamber is at an ultra-low state to avoid the severe combustion of alloy powder.

(2) In the relatively low laser powerp rocess range, the metallurgical bonding between coating and substrate is realized by optimizing the process, and the initiation of liquefaction or ductile crack is controlled.

(3) During the cladding process, the dust in the gas environment above the molten pool is continuously extracted and removed from the inert bin to reduce the dust content and prevent the dust from being wrapped into the coating.

Table.1 Test material composition(mass fraction/%)

Material composition	Zn	Nd	Zr	Ni	Cu	Mg
Substrate	0.10~0.70	2.00~2.80	0.40~0.52	0.01~0.03	0.10~0.15	Bal
Cladding layer	0.12~0.58	2.06~2.87	0.42~0.58			Bal

2.2 Realization of remanufacturing process

Before the experiment, the loose part of the magnesium alloy was removed by wire cutting. The magnesium alloy gearbox structure after loose part removal was shown by Fig. 1. The ZM6 alloy substrate was polished with sandpaper to remove the rust and oxide film on the surface, and dry it after cleaning with acetone and alcohol. The ZM6 cladding alloy powder was placed in the DSZF-2 vacuum drying oven and dried at 100 ℃ for 2 hours [12–13]. The 10×10×5mm homogeneous ZM6 alloy gasket was preset on the back surface of the defect wire cutting groove to facilitate the cladding forming of the defect groove. The IPG-4000 fiber laser remanufacturing system was used in the experiment, and the coaxial powder feeding method was used in the inert gas chamber. Before the process, the argon was continuously filled into the chamber to reduce the oxygen content in the chamber. The laser cladding process experiment was carried out when the oxygen content in the chamber was lower than 100 ppm. The laser optimization process was adopted in the cladding process, the pulse laser power was 1.2 kW, the spot diameter was 3 mm, the scanning speed was 5mm/s, the powder feeding rate was 21.4 g/min, and the carrier gas flow is 3 L/min.

During the forming process, the average forming height of a single layer was about 1 mm, a total of 5 layers were formed, the total forming height was about 5 mm, the cladding was stopped between layers

for 2 min to carry out automatic smoking and dust removal in the chamber. The overall shape of the gearbox after laser remanufacturing is shown in Fig. 2.

3 Microstructure And Properties

3.1 Defect X-ray control

The remanufactured formed part was cut by wire cutting to make a 30×30×3mm size test block for industrial X-ray flaw detection. The flaw detection test results were shown by Fig. 3. It could be seen from the figure that there were no internal macro defects such as porosity or pores in the remanufactured part. There was little light dark difference between the remanufactured area and the original substrate, indicating that the ray transmission degree of this area was close to the original substrate. It was verified that the density and element difference between the remanufactured part and the original substrate were close.

3.2 Element content matching

In order to further verify the element distribution changes between the coating, interface and substrate, the element line scanning was carried out at the joint of interface and substrate. The test results of main element content and distribution were shown by Fig. 4. It was seen from Fig. 4 (a) that the content of Zr, Nd, Zn and other elements in the cladding alloy material was relatively constant. Although there were some content fluctuations for Mg element in the above areas, still the overall content remains stable. From the interface to the substrate, the mass content of Mg was fluctuated between 96.06%~96.78%, the Zr mass content was between 0.39%~0.40%, the Nd mass content was between 2.45%~3.09% and the Zn mass content was between 0.38%~0.44%. The test results show that, the content of the above main elements were not fluctuated significantly, and remained basically constant, which the consistency and uniformity of the content of main elements between the coating, interface and substrate were verified.

3.3 Cladding microstructure

The laser cladding layer and substrate microstructure of ZM6 alloy were shown by Fig. 5. As was seen from Fig. 5(a), there was an obvious interface fusion line between the cladding layer and the substrate, the grain structure was obviously finer than that of the substrate. This was mainly because the laser molten pool experienced rapid condensation from high temperature, which promoted the nucleation of fine grain structure. At the same time, the formation of fine grain structure was conducive to the improvement of hardness. The ZM6 alloy substrate was mainly composed of equiaxed grains with similar grain size. There was no obvious coarsening in the heat affected zone (HAZ), which was mainly because the ZM6 alloy was affected by laser cladding heat input. The phase transformation was not occurred. So the grain size was changed little. The segregation at the grain boundary of the base metal was obvious. In the semi melting zone (PMZ) between the heat affected zone and the cladding, there existed a trend of grain growth, that was mainly because there existed solid-state phase transformation process affected by heat-input. It can be seen by comparing Fig. 5 (b)~(d) that the cladding structure was

mainly composed of equiaxed grains, and relatively fine granular or microsphere strengthening phases were dispersed and precipitated in the grains. There was a certain difference in grain size from the top to the bottom of the layer. The top of the cladding was in direct contact with the air, with good heat dissipation conditions and large temperature gradient, forming a large undercooling degree, so that the conditions for refinement were prepared for grain structures. The heat dissipation conditions in the middle of the coating were relatively poor, hence the temperature gradient is relatively small, so that the grains have some certain conditions for growth and inoculation. The bottom of the coating was in direct contact with the substrate, and the temperature gradient was also relatively large, which also inhibited the trend of grain growth to a certain extent.

3.4 Grain refinement and strengthening phase precipitation

The XRD phase analysis test results of the layer were shown in Figure 6. As the Figure 6 showed, the layer were mainly composed of hexagonal magnesium, zirconium and cubic magnesium oxide, but there was no Mg12Nd shown in the existing literature. It was mainly because the content of Mg12Nd was too small to be detected. However, the Zr was saturated precipitated in and between the crystals, the Zr element did not participate or hinder the analysis of solid solution, but its solid solution precipitation in α-Mg, which could refine grains and improve the strength of the cladding layer, and further improve the corrosion resistance of cladding.

4 Mechanical Properties Of Coating

4.1 Coating microhardness

In order to further verify the matching degree between the surface hardness of the coating and the substrate of ZM6 gearbox, especially whether there was excessive softening caused by forming heat input at the interface and heat affected zone, five test points at the top, middle, bottom, interface and cross-section of the substrate of single-layer forming coating were selected for measurement, and the average value was calculated after measurement. The experiment results were shown by Fig. 7. It could be seen from the figure that the microhardness near the top surface of the coating was the highest, reached the numerical value of 63.2$HV_{0.1}$. The microhardness value from the top of the coating to the interface showed a downward trend, the microhardness of the substrate was 52.3$HV_{0.1}$. The microhardness distribution from the top of the coating to the interface was between 63.2~56.4$HV_{0.1}$. The microhardness of the heat affected zone was about 56.4~54.2$HV_{0.1}$. The microhardness changes were relatively stable. This was mainly because the top forming layer was in direct contact with air. The layer has good heat dissipation conditions and large undercooling, which was conducive to the refinement of grain structure and the improvement of microhardness. Except for the top forming layer, the heat accumulation effect of other coatings was more significant, the grain morphology was relatively coarse, and the microhardness decreased. Although the hardness at the interface and heat affected zone decreased further, it was still higher than that of the substrate.

4.2 Friction and wear properties of coatings

The ball-disk contact reciprocating friction and wear test was carried out with NANOVEA friction and wear tester. The experiment was carried out under the condition of normal temperature and no lubrication. The Ø 6mm GCr15 steel ball was adopted as the friction pair, the loading force was 5N, the loading frequency was 2Hz and the loading time was 15min. After the experiment, the weight of the sample was reduced by 6.1mg, and the test results were shown by Fig. 8. It could be seen from the figure that, during the whole experiment process, the friction coefficient curve showed an overall trend of slow increase in the early stage, stable in the middle stage and slight increased in the later stage. At the initial stage of wear, the hardness of the friction pair was higher than that of the ZM6 magnesium alloy sample. The micro protrusions on the surface of the friction pair weared the magnesium alloy surface and produce furrows, fractures or fragments. The furrow shape would be stable in a relatively short period of time. In this stage, the friction coefficient increased, and the friction coefficient was mainly distributed between 0.26 and 0.34. Then the experiment entered the relatively stable friction equilibrium stage between the friction pair and the magnesium alloy surface. At this stage, the friction coefficient was little changed, and the friction coefficient was stablely between 0.32 and 0.38. As the friction continued, the surface wear of ZM6 magnesium alloy further intensified, resulting in the further increase of the friction coefficient, which reached between 0.36 and 0.42. This was mainly because a thin layer of magnesium alloy was adhered to the surface of the friction couple formed by the magnesium alloy coating and GCr15 steel ball, which adhered to the magnesium alloy sample and increases the friction coefficient.

4.3 Three point bending properties

In order to verify the three-point bending performance of ZM6 alloy laser cladding layer, the ZM6 magnesium alloy layer with sufficient size were prepared by cladding. The three-point bending specimens were cut according to the international standard Yb/T 5349-2014 test standard for impact properties of welded specimens. The transverse spacing of sampling positions of each sample was 50 mm. The upper surface of the cut sample was 0.3mm away from the upper surface of the coating, and the lower surface of the sample was 0.2mm away from the substrate surface. Five three-point bending test samples of the coating were cut, and the number of coating samples was 1~ 5. At the same time, 5 three-point bending test samples of the substrate were cut as the comparison group, with the substrate number of 6 ~ 10. The overall macro morphology of the samples after cutting were shown by Fig. 9.

When bending, ensure that the sample was placed straight, and the bending indenter was faced towards the middle of the sample. The three-point bending test of ZM6 magnesium alloy coating at room temperature was carried out by WDW-3100 universal mechanical testing machine. The experimental indenter was pressed at a rate of 0.5 mm/min at room temperature of 26 ℃. The test results were shown in Tab.2.

Tab.2 The verification datas of three point bending test for ZM6 magnesium alloy

Sample number	Maximum load F/N	Bending strength σ_f/ MPa	Sample number	Maximum load F/N	Bending strength σ_f/ MPa
1	158	214	6	176	230
2	167	220	7	182	237
3	152	205	8	172	226
4	169	223	9	180	236
5	170	224	10	178	234

According to the data in Table 2, the maximum bending load borne by ZM6 laser cladding layer was 152~167N, and the bending strength was distributed in 205~220 MPa. The maximum load of ZM6 substrate was 172~182N, and the bending strength was distributed at 226~237MPa. Although the bending strength of the coating was slightly lower than that of the substrate due to the influence of laser cladding heat input, the bending strength was still about 90.7~92.8% of the substrate, which still meeted the remanufacturing requirements, and the mechanical properties were not lower than 80% of the original.

5 Conclusions

(1) The optimum preparation process of laser cladding layer of ZM6 magnesium alloy under ultra-low oxygen content was studied. The oxygen content is controlled below 100 ppm, the pulse laser power is 1.2kW, the spot diameter is 3mm, the scanning speed is 5mm/s, the powder feeding rate is 21.4g/min, and the carrier gas flow is 3L/min.

(2) It is verified by X-Ray flaw detection and interface element line scanning that the contents of Zr, Nd, Zn and other elements in the coating and substrate are relatively constant. From the interface to the substrate, the mass content of Mg fluctuates between 96.06%~96.78%, Zr is between 0.39%~0.40%, Nd is between 3.09%~2.45% and Zn is between 0.44% ~ 0.38%.

(3) The grain structure of the coating is obviously finer than that of the substrate, which is mainly composed of equiaxed grains. Relatively fine granular or microsphere strengthening phases are dispersed in the grains, which are mainly composed of α-Mg phase and Zr element composition. The microhardness of the top surface of the coating is the highest, reaching 63.2$HV_{0.1}$. The microhardness from the top of the coating to the interface shows a downward trend, and the microhardness of the matrix is 52.3$HV_{0.1}$. The microhardness distribution from the top of the cladding to the interface is 63.2~56.4$HV_{0.1}$. The microhardness of the heat affected zone is about 56.4~54.2$HV_{0.1}$, and the microhardness changes in a relatively stable distribution state. The maximum bending load of the coating is 152~167N, and the bending strength is distributed in 205~220 MPa.

Declarations

Authors Contributions

Ren Weibin designed and performed relevant experiments, and wrote the manuscript; Wu Ruiyu provided some main experiment equipments; Wu Peng and Wang Yujiang completed part of the process experiments and processed the data; Ren Yuzhong and Li Yaping supervised the experiments and reviewed the manuscript.

Funding

This study was funded by the Fund of National Defense Science and Technology Key Laboratory of Equipment Remanufacturing Technology(No.ZX7Y201901SY00501-6142005180402), the Innovation Fund of National Commercial Aircraft Manufacturing Engineering Technology Research Center (COMAC-SFGS-2021-610).

Ethical approval The authors confirm that this work does not contain any studies with human participants performed by any of the authors.

Consent to publish The author grants the publisher the sole and exclusive license of the full copyright in the contribution, which license the publisher hereby accepts.

Competing interests The authors declare that they have no conflict of interest.

Data availability The authors declare that the data and the materials of this study are available within the article. The raw data are also available from the authors upon a reasonable request.

Code availability Not applicable.

References

1. Chen ZN, Jia HT, Geng XQ, Chen X, Zhang S (2020) (2020) 3-D distribution characteristics of the micro-defects in the PEO coating on ZM6 mg-alloy during corrosion. CORROS SCI. https://doi.org/10.1016/j.corsci.2020.108821
2. Zhang CL, Zhang F, Song L, Zeng RC, Li SQ, Han EH (2017) Corrosion resistance of a superhydrophobic surface on micro-arc oxidation coated Mg-Li-Ca alloy. J Alloys Compd. https://doi.org/10.1016/j.jallcom.2017.08.159
3. Aravind S, Ragupathi P, Vignesh G (2020) Numerical and experimental approach to eliminate defects in al alloy pump- crank case processed through gravity die casting route. Materials Today: Proceedings.https://doi.org/10.1016/j.matpr.2020.07.365
4. Li XB, Guo ZP, Xiong SM (2017) Influence of meltflow on the formation of defect band in high pressure diecasting of AZ91D magnesium alloy. Mater Charact. https://dx.doi.org/10.1016/j.matchar.2017.05.009

5. Song JH, Murugan Subramani, Chao CC (2021) Effect of hybrid reinforcement on microstructure and mechanical properties of az61 magnesium alloy processed by stir casting method. Compos Commun. https://doi.org/10.1016/j.coco.2021.100772
6. Miroslav Sahul M, Sahulb J (2016) Lokajb Effect of surface layer on the properties of AZ31 magnesium alloy welded joints. Materials Today: Proceedings. https://doi.org/10.1016/j.matpr.2016.03.015
7. Wahba M, Kawahito Y, Katayamac S (2011) Laser direct joining of AZ91D thixomolded Mg alloy and amorphous polyethylene terephthalate. J Mater Process Tech. https://doi.org/10.1016/j.jmatprotec.2011.01.021
8. GAO Y, Xiong DS, Wang CS (2009) Influences of laser powers on microstructure and properties of the coatings on the AZ91HP magnesium alloy. https://doi.org/10.1016/S1006-7191(08)60085-X. ACTA METALL SIN-ENGL.
9. Zheng Y, Xu L, Wang GH, Chen YB (2015) Microstructure and properties of ZM6 magnesium alloy repair welding. WELD J 12:63–66
10. Wang X, Yang C, Wang JC (2010) TIG repair welding process of ZM6 magnesium alloy casting. WELD J 31(9):33–38
11. Li XX, Li ZY, Zhu RD, Xue FF (2014) Effects of cladding materials and process parameters on defects of laser cladding layer of magnesium alloy. Welding Technology 43(11):5–8
12. Ren WB, Dong SY, Xu BS, Yan SX, Fang JX (2017) Dynamic deformation law and experimental optimization of FV520 (B) steel blade Laser Remanufacturing. J Harbin Inst Technol https://doi.org/10.11918 /j.issn.0367-6234.201512038
13. Ren WB, Dong SY, Xu BS, Yan SX, Wang YJ, Yan SX (2015) Optimization of laser remanufacturing process and forming repair of FV520 (B) steel blade simulator. J MATER ENG. https://doi.org/10.11868/j.issn.1001-4381.2015.01.002
14. Ren WB, Zhuang BL, Lei WN, Cao QL (2021) Microstructure and performance evolution of Ti-6Al-4 V alloy coating by laser cladding and laser shocking composite remanufacture. Opt Laser Technol. https://doi.org/10.1016/j.optlastec.2021.107342
15. Ren WB, Zhou JY, Zhang SR, Xu BS (2019) Shape and performance control of K418 superalloy impeller remanufactured by pulsed laser. Rare Metal Mat Eng 48(10):3315–3319
16. Ren WB, Cao QL, Zhuang BL, Chen SX (2021) Process and mechanical properties of variable radius FeCrNiCu alloy cylinder formed by pulsed laser cladding. Rare Metal Mat Eng 50(3):973–978

Figures

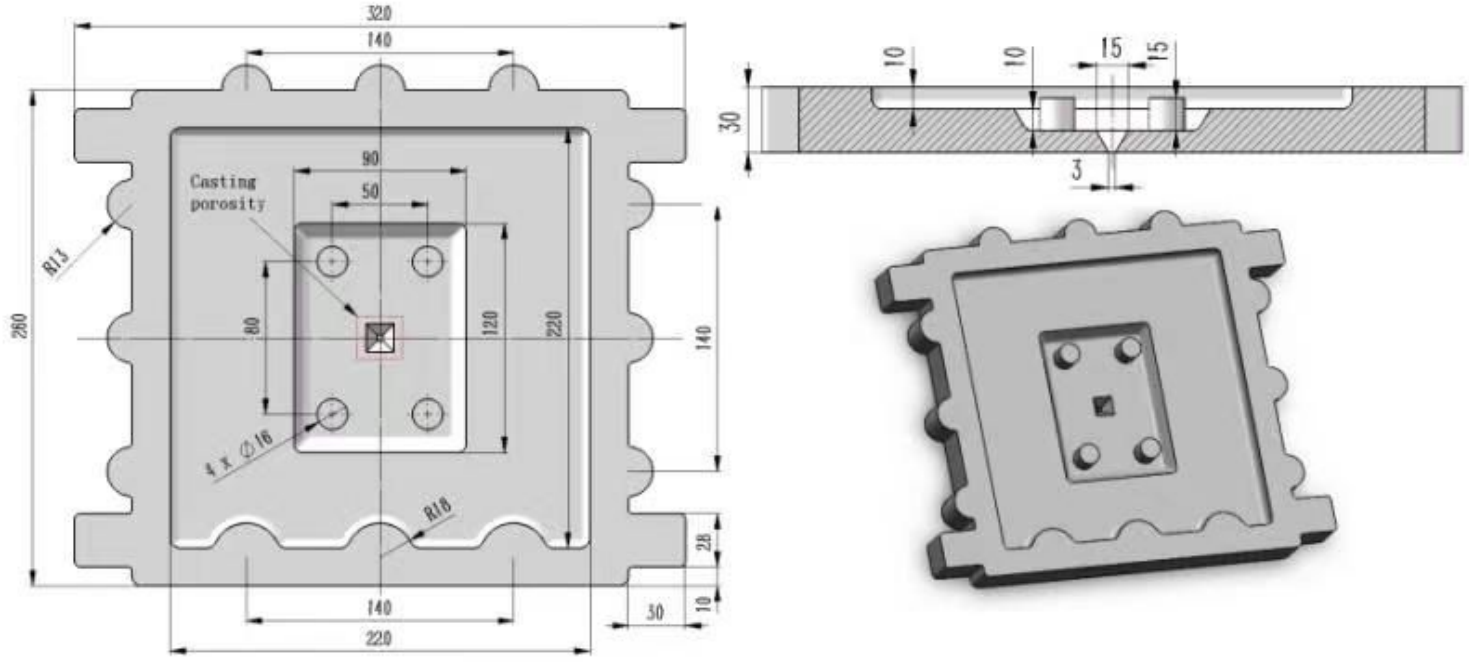

Figure 1

Dimension structure and defect location of ZM6 alloy gearbox

Figure 2

The ZM6 magnesium alloy gearbox after laser remanufacture

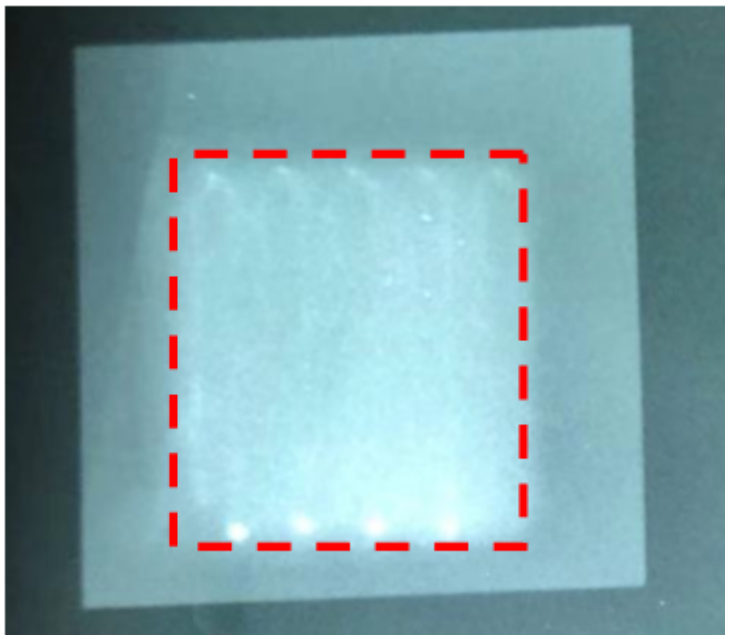

Figure 3

The X-ray inspection test image of the laser remanufacture area

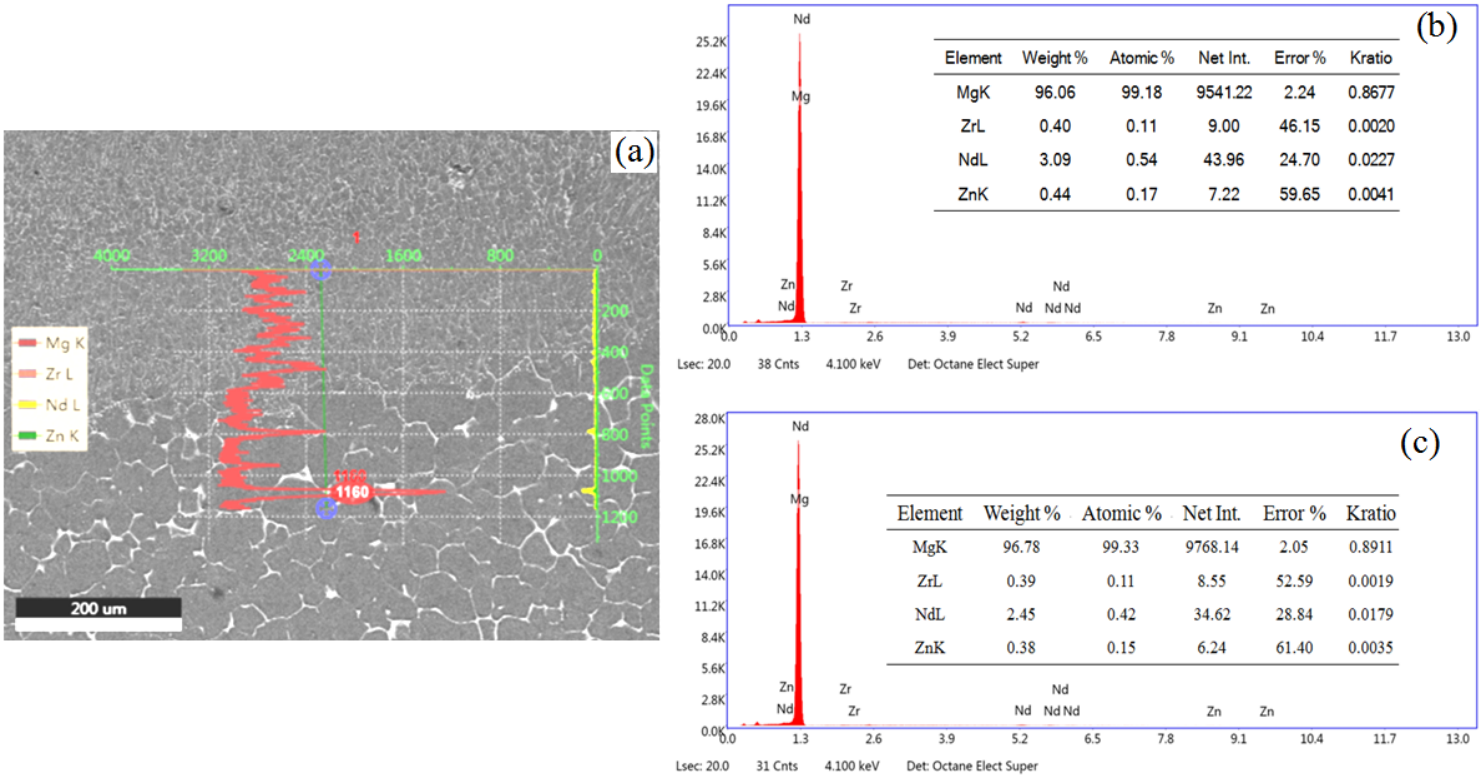

Figure 4

The main element content and distribution

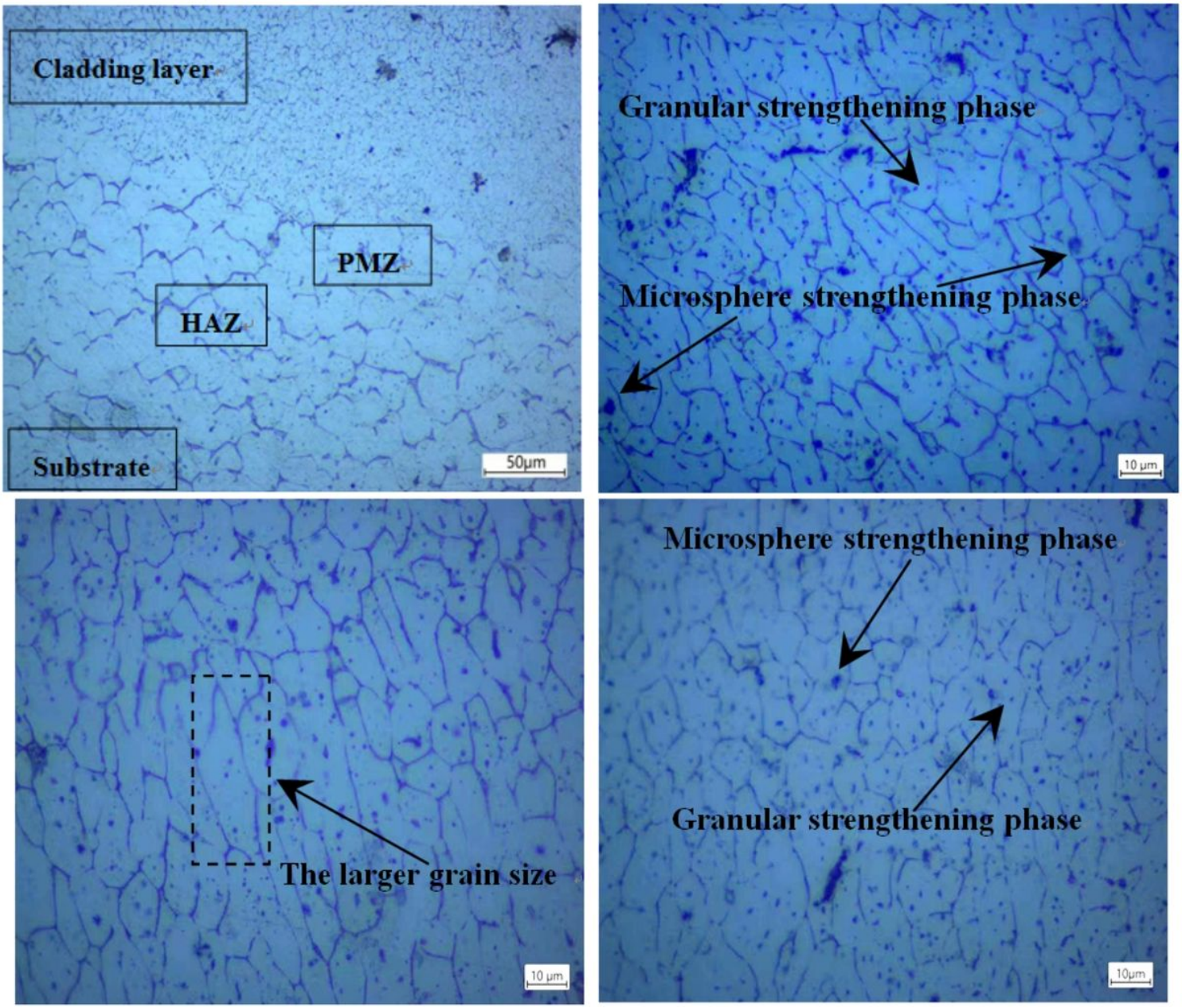

Figure 5

The laser cladding layer and matrix metallographic structure of ZM6 magnesium alloy

(a) The metallographic structure of the interface (b) The metallographic structure of the top cladding layer

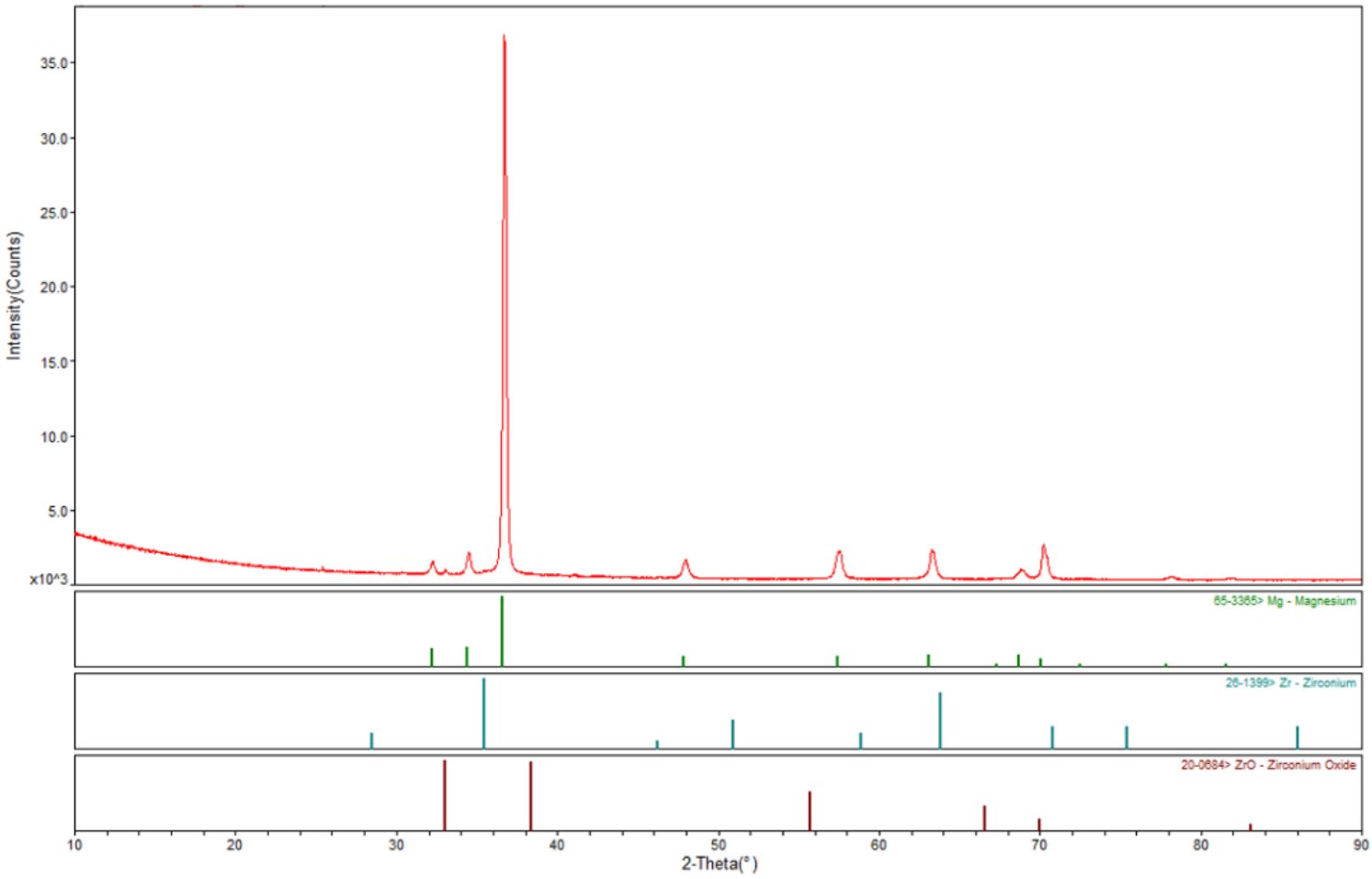

Figure 6

The composition of the precipitated strengthening phases of the cladding layer

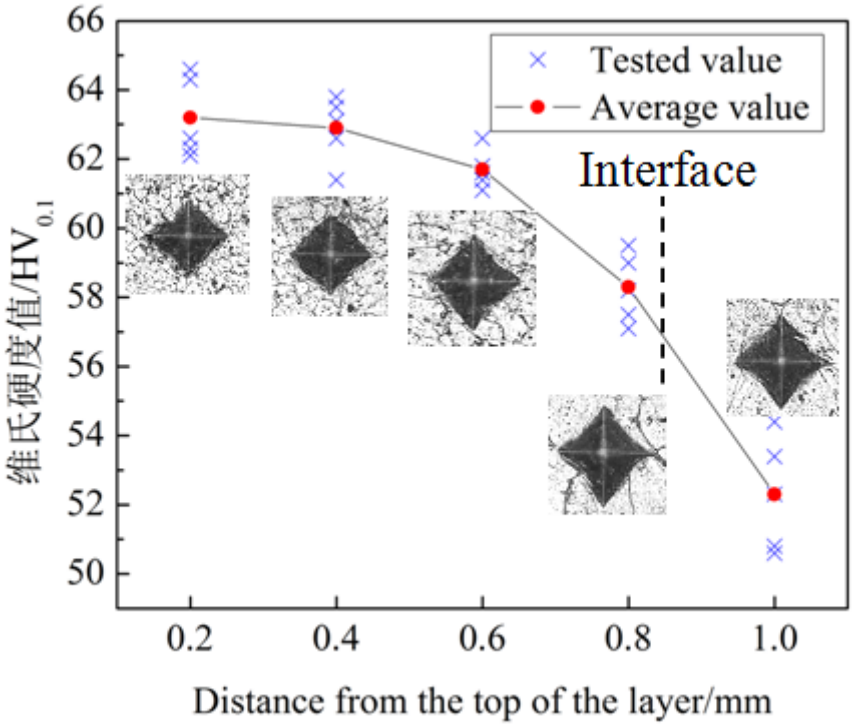

Figure 7

The microhardness distribution of the layer and the layer of ZM6 magnesium alloy

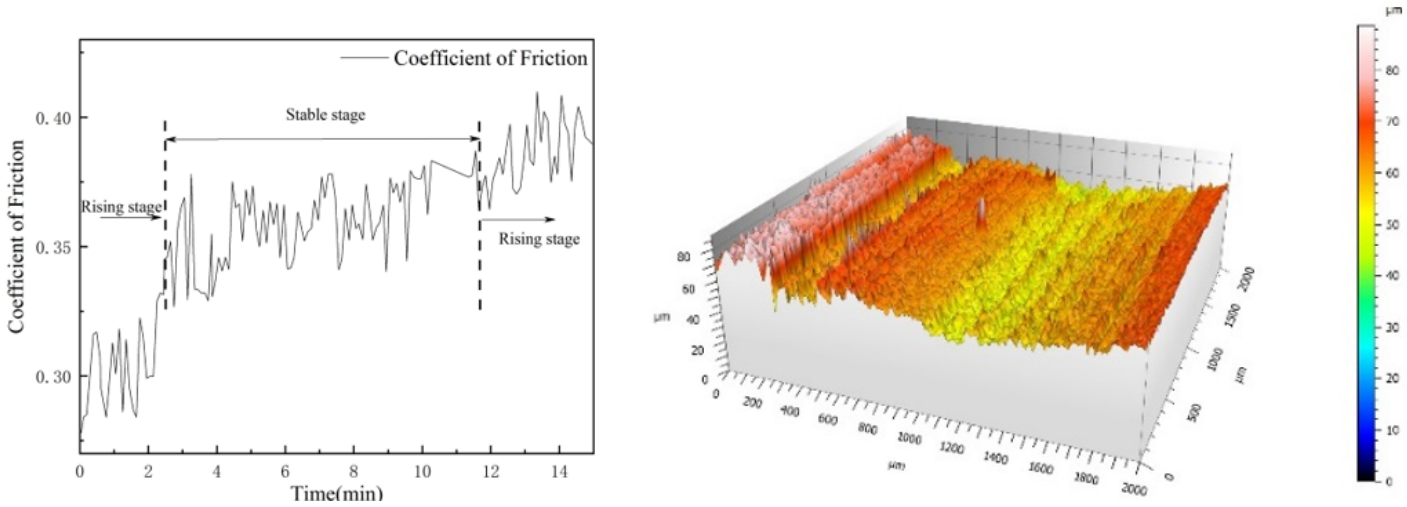

Figure 8

Friction coefficient curves and surface morphologies of coating for friction and wear

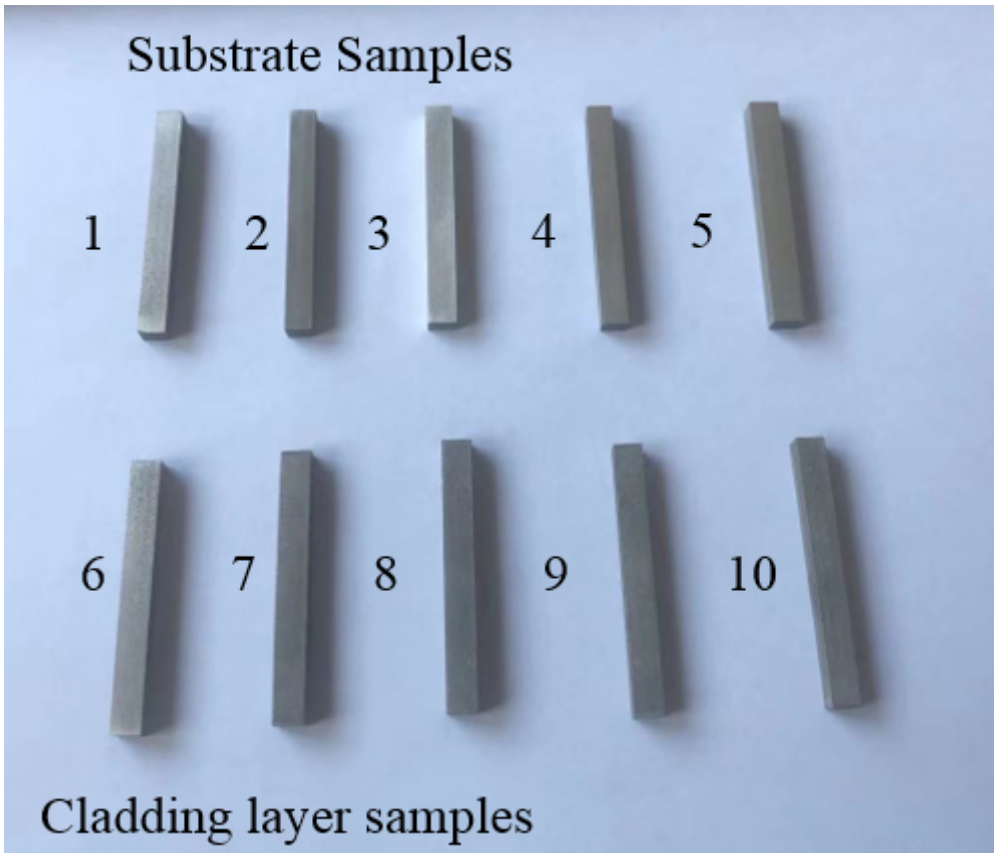

Figure 9

The three-point bending specimens of laser cladding for ZM6 magnesium alloy